Physics Letters B 785 (2018) 615–620

Contents lists available at ScienceDirect

Physics Letters B

www.elsevier.com/locate/physletb

# Neutron-hole states in $^{131}$Sn and spin-orbit splitting in neutron-rich nuclei

R. Orlandi [a,b,c,d,*], S.D. Pain [e], S. Ahn [f], A. Jungclaus [b], K.T. Schmitt [f], D.W. Bardayan [e], W.N. Catford [g], R. Chapman [c,d], K.A. Chipps [h,e], J.A. Cizewski [i], C.G. Gross [e], M.E. Howard [i], K.L. Jones [f], R.L. Kozub [j], B. Manning [i], M. Matos [k], K. Nishio [a], P.D. O' Malley [i], W.A. Peters [l], S.T. Pittman [e], A. Ratkiewicz [i], C. Shand [g,i], J.F. Smith [c,d], M.S. Smith [e], T. Fukui [m,n], J.A. Tostevin [g,o], Y. Utsuno [a]

[a] Advanced Science Research Center, Japan Atomic Energy Agency, Tokai, Ibaraki, 319-1195, Japan
[b] Instituto de Estructura de la Materia (IEM), CSIC, Madrid, E-28006, Spain
[c] School of Engineering and Computing, University of the West of Scotland, Paisley, PA1 2BE, UK
[d] The Scottish Universities Physics Alliance (SUPA), UK
[e] Physics Division, Oak Ridge National Laboratory, Oak Ridge, TN 37831, USA
[f] Department of Physics and Astronomy, University of Tennessee, Knoxville, TN 37996, USA
[g] Department of Physics, University of Surrey, Guildford, GU2 7XH, UK
[h] Physics Department, Colorado School of Mines, Golden, CO 80401, USA
[i] Department of Physics and Astronomy, Rutgers University, New Brunswick, NJ 08903, USA
[j] Department of Physics, Tennessee Technological University, Cookeville, TN 38505, USA
[k] Department of Physics and Astronomy, Louisiana State University, Baton Rouge, LA 70803, USA
[l] Oak Ridge Associated Universities, Oak Ridge, TN 37831, USA
[m] Nuclear Data Center, Japan Atomic Energy Agency, Tokai, Ibaraki 319-1195, Japan
[n] Istituto Nazionale di Fisica Nucleare, Complesso Universitario di Monte S. Angelo, Via Cintia, I-80126 Napoli, Italy
[o] Department of Physics, Tokyo Institute of Technology, Meguro, Tokyo, 152-8551, Japan

ARTICLE INFO

*Article history:*
Received 23 May 2018
Received in revised form 13 July 2018
Accepted 3 August 2018
Available online 7 August 2018
Editor: D.F. Geesaman

*Keywords:*
Nuclear structure
Spin-orbit interaction
Transfer reactions
Doubly-magic nuclei
Shell model

ABSTRACT

In atomic nuclei, the spin-orbit interaction originates from the coupling of the orbital motion of a nucleon with its intrinsic spin. Recent experimental and theoretical works have suggested a weakening of the spin-orbit interaction in neutron-rich nuclei far from stability. To study this phenomenon, we have investigated the spin-orbit energy splittings of single-hole and single-particle valence neutron orbits of $^{132}$Sn. The spectroscopic strength of single-hole states in $^{131}$Sn was determined from the measured differential cross sections of the tritons from the neutron-removing $^{132}$Sn(d,t)$^{131}$Sn reaction, which was studied in inverse kinematics at the Holifield Radioactive Ion Beam Facility at Oak Ridge National Laboratory. The spectroscopic factors of the lowest $3/2^+$, $1/2^+$ and $5/2^+$ states were found to be consistent with their maximal values of $(2j+1)$, confirming the robust $N=82$ shell closure at $^{132}$Sn. We compared the spin-orbit splitting of neutron single-hole states in $^{131}$Sn to those of single-particle states in $^{133}$Sn determined in a recent measurement of the $^{132}$Sn(d, p)$^{133}$Sn reaction. We found a significant reduction of the energy splitting of the weakly bound $3p$ orbits compared to the well-bound $2d$ orbits, and that all the observed energy splittings can be reproduced remarkably well by calculations using a one-body spin-orbit interaction and a Woods–Saxon potential of standard radius and diffuseness. The observed reduction of spin-orbit splitting can be explained by the extended radial wavefunctions of the weakly bound orbits, without invoking a weakening of the spin-orbit strength.



The spin-orbit (SO) interaction, which arises from the coupling of the orbital motion of a particle with its intrinsic spin, affects the properties of a diverse number of systems, such as atomic electrons [1], carbon nanotubes [2] or quantum gases [3]. In nuclear physics, the SO interaction is often described in the mean-field approximation, as a one-body potential term proportional to the derivative of the nuclear density [4]. In this model, the SO poten-

* Corresponding author at: Advanced Science Research Center, Japan Atomic Energy Agency, Tokai, Ibaraki, 319-1195, Japan.
*E-mail address:* orlandi.riccardo@jaea.go.jp (R. Orlandi).

https://doi.org/10.1016/j.physletb.2018.08.005
0370-2693/

tial strength is empirically determined from the energy difference, $\Delta_{so}$, between either proton or neutron orbits of angular momentum $\ell > 1$, which split into "$j$-upper" $j_> = \ell + 1/2$ and "$j$-lower" $j_< = \ell - 1/2$ partner orbits. The inclusion of a SO potential term in the nuclear shell-model Hamiltonian [5] was paramount to reproduce the established magic numbers and the shell gaps. In recent years, the SO interaction has elicited new interest due to its implications for the structure of neutron-rich nuclei, which exhibit dramatic structural changes away from the valley of stability [6–8]. Many of these changes have been attributed to the nucleon–nucleon tensor force [9], which acts with opposite sign on $j_>$ and $j_<$ orbits. The contribution of the SO interaction, however, still needs to be clarified. Various theoretical approaches, such as relativistic mean-field [10] or calculations based on realistic nucleon–nucleon potentials [11], predict a weakening of the SO interaction in neutron-rich nuclei, which would lead to smaller SO energy splittings ($\Delta_{so}$). Conversely, Hamamoto et al. [12] predict the $\Delta_{so}$ of weakly bound orbits in light, neutron-rich nuclei to decrease due to the extended radial wavefunctions of neutron orbits, with no reduction of the SO potential strength. Experimentally, the authors of Ref. [13] questioned whether a weakened SO interaction could provide a possible explanation for the shifts of single-particle energies determined in their work for the odd-mass Sb isotopes; however, the effects of the tensor force can also convincingly describe the same data [14]. Recently, Burgunder et al. [15] studied the behavior of states with a strong single-particle character based on the $2p_{3/2} - 2p_{1/2}$ neutron orbits outside of the $N = 20$ closed shell, populated via neutron-adding reactions in $N = 21$ isotones $^{41}$Ca, $^{37}$S and $^{35}$Si. They derived a 25% reduction in the $\Delta_{so}$ of the $2p$ orbits between $^{37}$S and $^{35}$Si, and attributed this reduction to the different strength of the two-body SO term of the matrix elements between protons in the $2s_{1/2}$ and neutrons in the $2p_{3/2}$ and $2p_{1/2}$ orbits. An alternative explanation of the same data has been given by Kay et al. [16]: they attribute instead the reduced $\Delta_{so}$ to the low binding energy of the $2p$ states, and describe the data using a one-body Woods–Saxon potential without assuming a reduced SO potential strength, in analogy to Ref. [12]. The comparison of different nuclei, $^{37}$S and $^{35}$Si, requires, in the approach of Ref. [15], to isolate the effects of the SO interaction from those of the tensor force and, in Ref. [16], that the depth of the potential be adjusted to reproduce the different nuclear binding energies of the $^{35}$Si and $^{37}$S isotopes.

In this Letter, we present an original viewpoint which removes the uncertainties linked to the comparison of different systems, by analyzing the $\Delta_{so}$ of different pairs of neutron partner orbits in the same neutron-rich, doubly magic nucleus, $^{132}$Sn. The $\Delta_{so}$ values of neutron orbits above and below the shell gap at $N = 82$ were determined, respectively, from the neutron-adding $^{132}$Sn(d, p)$^{133}$Sn reaction [17] and the neutron-removing $^{132}$Sn(d, t)$^{131}$Sn reaction, described in this work. The comparison of different orbits in $^{132}$Sn reveals a reduced energy splitting of the weakly bound $3p$ states compared to the well-bound $2d$ states. A similar but smaller reduction is also exhibited by the weakly bound $2f$ orbits. All $\Delta_{so}$ values can be remarkably well reproduced using a one-body SO potential, in the spirit of Refs. [12] and [16], using the same SO potential strength for all orbits.

In a simplified picture, the low-lying states of $^{133}$Sb, $^{133}$Sn, $^{131}$In and $^{131}$Sn (see Fig. 1) are expected to correspond to single-particle or single-hole proton and neutron configurations across the $Z = 50$ and $N = 82$ shell gaps. This assumption needs to be tested by determining their spectroscopic factors (S), a meaningful indicator of the purity of their single-particle(hole) character. Prior to this work, the spectroscopic factors of single-particle states in $^{133}$Sn were determined [18] for levels based on the $2f$ and $3p$ orbits above the $N = 82$ shell gap (see Fig. 1), 14 years after the first

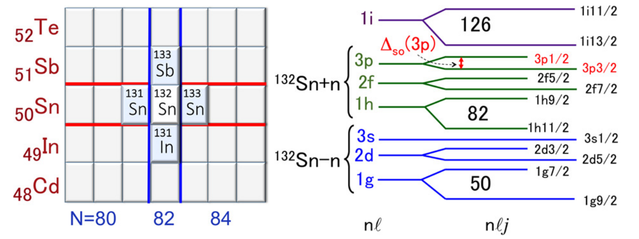


**Fig. 1.** Left: section of the nuclear chart showing the location of $^{132}$Sn and its neighbors along the $Z = 50$, $N = 82$ magic numbers. Right: neutron single-particle orbits expected to be populated via the $^{132}$Sn(d, p)$^{133}$Sn (stripping) and $^{132}$Sn(d, t)$^{131}$Sn (pick-up) reactions. The energy difference between the $3p$ SO partner orbits, $\Delta_{so}(3p)$, is schematically highlighted by the double-headed arrow.

$\beta$-decay study of $^{133}$Sn [19]. Analogous single-particle states, lying between 2.6 and 4.7 MeV, were also populated in $^{131}$Sn via the $^{130}$Sn(d, p) reaction [20]. While considerable efforts have been expended in studying single-neutron states in heavy neutron-rich unstable nuclei via neutron-adding reactions at Coulomb-barrier energies [17,20–27], there are no transfer reaction studies of hole states around $^{132}$Sn. This omission is largely due to the experimental challenges of measuring pick-up reactions on heavy nuclei in inverse kinematics, which requires very fine angular resolution in order to resolve neighboring states, due to the steep, double-valued energy vs. angle reaction kinematics [28]. Low-energy excitations in $^{131}$Sn are mainly known from $\beta$-decay studies [29], with the sole exception of the 332-keV state in $^{131}$Sn, also populated via the $^{132}$Sn($^{9}$Be, $^{10}$Be)$^{131}$Sn reaction [21] at sub-Coulomb energy. The low-lying states of $^{133}$Sb and $^{131}$In were only observed in $\beta$-decay [30–32]. The $^{131}$Sn data presented in this Letter come from the first (d, t) reaction performed in this region of heavy, neutron-rich nuclei.

Further interest in studying the energies of single-particle states near $^{132}$Sn is due to their importance for determining abundances from rapid neutron-capture ($r$-process) nucleosynthesis models, which are sensitive to neutron-capture cross sections on currently inaccessible nuclei [33]. A weakening of the SO interaction would lead to significant shifts in the single-particle energy spectrum, and predicting where these states lie in nuclei that cannot be studied experimentally is crucial. Direct-Semi Direct (DSD) neutron capture, which is considered to be the dominant mechanism beyond shell closures [34], is critically sensitive to the energies of low-$\ell$ single-particle states, which could display a reduced energy splitting. Variations in DSD cross sections of 2–3 orders of magnitude have been shown to arise from different nuclear structure models, based largely on whether the low-$\ell$ states are predicted to be bound to neutron decay [20].

In the present work, the $^{131}$Sn experiment was performed at the Holifield Radioactive Ion Beam Facility (HRIBF) at Oak Ridge National Laboratory. Low-lying states in $^{131}$Sn were populated via the $^{132}$Sn(d, t)$^{131}$Sn reaction (ground-state Q value: −1.096(4) MeV [35]) in inverse kinematics. The radioactive $^{132}$Sn ($T_{1/2} = 39.7(8)$ s [36]) beam was produced via the proton-induced fission of $^{238}$U in a UCx target, extracted using the isotope separation online (ISOL) technique, and accelerated by the 25-MV ORNL Tandem electrostatic accelerator to 580 MeV ($\sim 4.4$ MeV/u). The beam purity and average intensity, measured using a fast ionization chamber [37] placed downstream of the target chamber, were $\sim 99\%$ and $1.2 \cdot 10^{4}$ particles per second, respectively. The beam impinged on thin films of deuterated polyethylene ($C_2D_4$) [38]. Two targets were used: the initial 214-μg/cm$^2$-thick film was replaced after 40 hours of beamtime with a thicker (350-μg/cm$^2$) one, which almost doubled the counting rates without affecting significantly the energy resolution. The target thicknesses were measured from the energy loss of alpha particles from a $^{244}$Cm

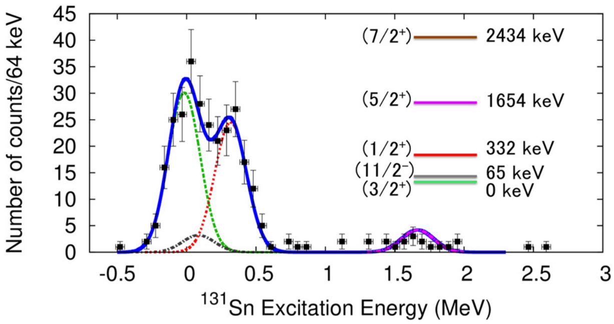


**Fig. 2.** $^{131}$Sn excitation-energy spectrum deduced from tritons detected with Super-ORRUBA between 36 and 50 degrees in the laboratory frame. The blue line is the sum of the Gaussian fits to the 0-, 65-, 332- and 1654-keV peaks. (Inset) Lowest-lying states in $^{131}$Sn [41].

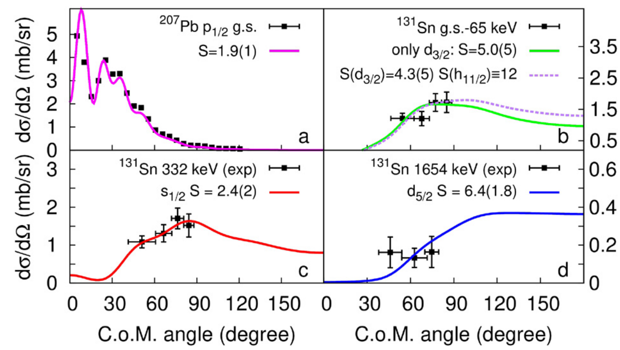


**Fig. 3.** Measured differential cross sections fitted by calculated DWBA calculations for the ground state of $^{207}$Pb (a) [49] and for states in $^{131}$Sn (b–d). See text for details.

alpha source, with an overall error $<10\%$. The experiment lasted nearly five days.

The SuperORRUBA array of segmented Si telescopes [39] was used to detect tritons from the (d, t) reaction. The array comprised of seven ΔE-E telescopes from the ORRUBA array [40] to identify the light ejectiles and four additional E detectors to monitor elastically-scattered deuterons for beam normalization. The respective thickness was 65 μm for ΔE and 1000 μm for E detectors. The telescopes were placed at a radial distance of 123 mm from the target. The large segmentation of the E detectors (64 strips perpendicular to the beam direction) combined with the 8-fold segmentation (parallel to the beam direction) of the ΔE detectors, resulted in an average resolution of 0.28 degrees in polar angle. The angular range covered by the telescopes and two of the E detectors was $\sim 35$–50 degrees in the laboratory frame, while the two remaining E detectors were placed close to 90 degrees (0 degrees in the center-of-mass system), where the elastic scattering cross section is largest and closest to the Rutherford cross section. Tritons were discriminated from other charged particles by their ΔE-E energy deposition behavior on a particle-identification plot [28].

For each detected triton, the corresponding excitation energy of $^{131}$Sn was calculated using binary-reaction kinematics. The resulting excitation-energy spectrum is shown in Fig. 2, together with the low-energy levels of $^{131}$Sn. The configurations of these states, deduced from $\beta$-decay [29], are generally assigned, in ascending order, to a single hole in the neutron $d_{3/2}$, $h_{11/2}$, $s_{1/2}$, $d_{5/2}$ and $g_{7/2}$ orbits. The FWHM energy resolution of the calculated excitation energy is $\sim 240$ keV for individual telescopes and $\sim 270$ keV for the summed spectrum in Fig. 2, sufficient to resolve the stronger peaks, but not the 0–65-keV doublet. The two largest peaks in Fig. 2 correspond to the 0–65-keV doublet [29] and the 332-keV excited states, respectively. Most of the counts in the lower energy peak are likely to come from the population of the $d^{-1}_{3/2}$ state, since the $h^{-1}_{11/2}$ state is unfavored by the large angular momentum transfer ($5\hbar$). In the fit, the fixed parameters were sigma, the centroid of the 65-keV peak and the ratio of the amplitudes of the 0- and 65-keV states. The amplitude ratio was determined from the integrated cross-sections for the $d_{3/2}$ and $h_{11/2}$ orbits calculated in the distorted-wave Born approximation (DWBA) over this angular range, assuming full occupancy for both orbits. For the $(3/2^+)$ and $(1/2^+)$ states, the current assignments are consistent with the differential cross sections measured in this work. A smaller peak, corresponding to the 1654-keV ($d^{-1}_{5/2}$) state, can be seen at 1665(116) keV. Its low cross-section is due to the more negative Q-value, $-2.764$ MeV.

Triton angular distributions for the 0–65-doublet, 332- and 1654-keV states were extracted from Gaussian fits to the excitation energy spectrum at different angles. For the unresolved doublet only one Gaussian was fitted and the data analyzed as the summed distributions of $d_{3/2}$ and $h_{11/2}$ orbits. The triton angular distributions were converted to absolute cross sections using the normalization determined from the elastic scattering of deuterons from the target [18]. Deviations from the Rutherford scattering differential cross section at these energies and angles are less than 5%. This technique greatly reduces the uncertainties in the number of target deuterons and beam ions (bypassing the need to know the initial target thickness and content, and directly accounts for beam-induced carbonization of the foil) [38]. The triton angular distributions were compared with DWBA calculations, using the code TWOFNR [42]. Empirical spectroscopic factors are deduced by scaling the DWBA distributions to the experimental data. In the case of pick-up reactions, like the present (d, t) case, S indicates the level of filling of the orbit from which the neutron was removed; so, in a simple shell model picture, S lies between 0 and $2j+1$.

The DWBA calculations carried out in this work treat the finite range of the (d, t) transition potential using the local energy approximation [43], with a finite-range parameter 0.845 fm, and a $<\mathrm{d}|\mathrm{t}>$ vertex normalization constant, $D_0$, of $-163$ MeV fm$^{3/2}$ [44,45]. Perey–Buck-type non-localities [46] are included in the deuteron and triton distorting potentials with non-locality parameters of 0.54 and 0.25 fm, respectively. The deuteron and triton optical model potentials of Daehnik et al. [47] and Becchetti (as described in [48]) were employed. The radius and diffuseness parameters of the Woods–Saxon potential wells used for the neutron bound states were 1.25 and 0.65 fm, respectively. The experimentally deduced spectroscopic factors provide a good indication of the relative spectroscopic strengths of the populated states.

Insight can also be gained by comparing the experimental spectroscopic factors with those of neutron single-hole states in, e.g., $^{207}$Pb [49,50], populated via (d, t) reactions on $^{208}$Pb, whose doubly magic nature is well known. Since the extraction of absolute values of spectroscopic factors is a long-debated issue in the analysis of transfer reactions, DWBA calculations for the $^{208}$Pb(d, t)$^{207}$Pb reaction were carried out to show the overall consistency. The same optical model potentials, vertex normalization constant and non-locality parameters were used for both the $^{131}$Sn and $^{207}$Pb calculations.

A summary of the theoretical and experimental angular distributions is shown in Fig. 3. The doubly magic character of $^{132}$Sn was unambiguously established by the (d, p) transfer reaction of Jones et al. [17,18]. The large spectroscopic factors extracted in this work for the 0-, 332- and 1654-keV states in $^{131}$Sn indicate that the $2d_{3/2}$, $3s_{1/2}$ and $2d_{5/2}$ neutron orbits below the $N=82$ shell gap are fully occupied, and further corroborate the doubly magic nature of $^{132}$Sn. Other optical model potentials [51–53] change by $\sim$ 10–20% the extracted spectroscopic factors, but yield the same picture.

The data for the $^{207}$Pb $p_{1/2}^{-1}$ ground-state shown in Fig. 3 (a) are from Ref. [49] (21.5 MeV deuteron beam energy). The distribution is well reproduced by the DWBA calculations with $S(3p_{1/2}) = 1.9(1)$ (only statistical errors are shown), indicating as expected full occupancy of the $p_{1/2}$ orbit. The $^{131}$Sn data are shown in Fig. 3(b–d). The distribution shown in Fig. 3 (b) is that of the unresolved 0–65-keV doublet in $^{131}$Sn. Two calculations are presented: pick-up from a pure $d_{3/2}$ state (solid line), yielding $S(d_{3/2}) = 5.0(5)$, and the summed-distribution of pick-up from both the $d_{3/2}$ and $h_{11/2}$ orbits (dashed line), which gives $S(d_{3/2}) = 4.3(5)$ when $S(h_{11/2}) \equiv 12$ is assumed. The differential cross section measured for the 332-keV state, in Fig. 3 (c), is consistent with the proposed $s_{1/2}^{-1}$ configuration [29]. The spectroscopic factor determined via sub-Coulomb transfer [21] was 4(3). The theoretical (d, t) reaction analysis, with better-determined potentials, provides a more stringent measurement, with $S(s_{1/2}) = 2.4(2)$. For the $d_{5/2}$ state, the $S(d_{5/2}) = 6.4(1.8)$ is consistent with full occupancy of the $d_{5/2}$ orbit in $^{132}$Sn and a pure hole configuration for the 1654-keV state in $^{131}$Sn. The $(7/2^+)$ state at 2343 keV was not observed. All extracted spectroscopic factors exhaust the full $2j+1$ spectroscopic strength and indicate within the error that the low-lying $s$ and $d$ excited states in $^{131}$Sn are good single-hole states. Having assessed their single-hole nature, the $\Delta_{so}$ for the $2d_{3/2}$ and $2d_{5/2}$ orbits can be taken as the energy difference between the ground and 1654-keV states. The SO energy splitting of the strongly bound $2d$ orbits is key to the following discussion, since it permits the determination of the strength of the SO potential in $^{132}$Sn. To better explain this point, and the observed differences of the $\Delta_{so}$ values, it is useful to include a reminder of the one-body potential description of the SO interaction.

A general definition of the average spherical nuclear potential for neutrons is given by [4]:

$$U(r) = V_0(r) + V_{ls}(r) = V_0 f(r) + V_{ls} r_0^2 \boldsymbol{\ell} \cdot \boldsymbol{s} \frac{1}{r}\frac{\partial}{\partial r} f(r), \quad (1)$$

where $V_0$ and $V_{ls}$ are respectively the central and SO potential strengths, and where $f(r)$ is a radial function of central Woods–Saxon type:

$$f(r) = \left[1 + \exp\left(\frac{r-R}{a}\right)\right]^{-1}, \quad (2)$$

where $R = r_0 A^{1/3}$ and $r_0$ and $a$ are the radius and diffuseness parameters. In this model, the SO interaction is of necessity a surface term. By approximating $V_{ls}(r)$ to a $\delta$ function at the nuclear surface [4],

$$\langle V_{ls}(r)\rangle \approx V_{ls}(\boldsymbol{\ell} \cdot \boldsymbol{s}) r_0^2 R \mathscr{R}^2(R) \quad (3)$$

where $\mathscr{R}(R)$ is the amplitude of radial neutron wavefunctions at the mean nuclear radius $R$. For orbits bound from a few MeV up to 10 MeV, the dimensionless quantity $R^3\mathscr{R}^2(R)$ is fairly independent of the specific orbit involved, and is on average 1.4 with 10–20% fluctuations. In this approximation, the SO energy shifts of bound states are approximately $1.4 V_{ls}(\boldsymbol{\ell} \cdot \boldsymbol{s}) A^{-2/3}$, similar to those observed in stable nuclei [4]. It follows that $\Delta_{so}$ increases linearly with $(\ell + 1/2)$, with the expectation that the quantity $\Delta_{so}/(\ell + 1/2)$ is nearly the same for strongly bound orbits.

The $\Delta_{so}$ values for the $3p$, $2d$ and $2f$ orbits in $^{132}$Sn are plotted as a function of $\ell$ in Fig. 4 (a), where the energies of the $p$ and $f$ orbits are from Ref. [17,19]. The experimental uncertainties for the tin data depend on possible unobserved states; however,

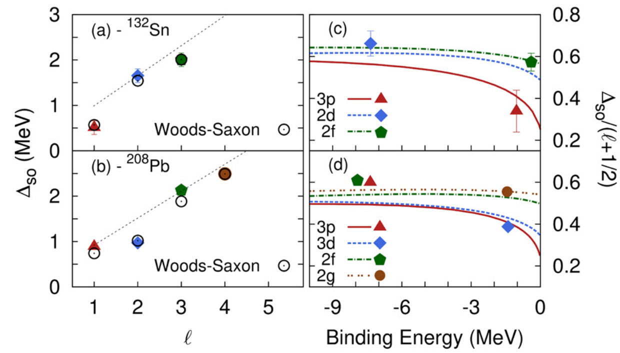


**Fig. 4.** (Left) $\Delta_{so}$ values vs. orbital angular momentum $\ell$ in $^{132}$Sn (a) and $^{208}$Pb (b). For $^{208}$Pb, the uncertainties are smaller than the size of the symbols. Experimental $\Delta_{so}$ (filled symbols) are compared with a linear $(\ell + 1/2)$ dependence (dashed line) and with Woods–Saxon calculations (open circles). The experimental values for $^{132}$Sn are from this work and Ref. [29] ($2d$), and from Ref. [19] ($3p$ and $2f$). For $^{208}$Pb, $\Delta_{so}$ values are from Ref. [54]. (Right) The quantity $\Delta_{so}/(\ell + 1/2)$, calculated for different orbits as a function of binding energy in $^{132}$Sn (c) and $^{208}$Pb (d). The experimental $\Delta_{so}$ values, represented by the symbols, are plotted vs the binding energy of the $j_<$ states.

the large spectroscopic factors revealed by both transfer measurements, and the doubly-magic character of $^{132}$Sn, indicate that a significant fragmentation of the single-hole strength among several levels is very unlikely, and an average uncertainty of $\pm$150 keV was adopted, from comparison with $^{208}$Pb and the discussion in Ref. [54].

The $(\ell + 1/2)$ proportionality is described by the straight line in Fig. 4 (a), scaled to the $\Delta_{so}$ of the $2d_{5/2}$ and $2d_{3/2}$ orbits, with respective binding energies of $-9.007(4)$ and $-7.353(4)$ MeV [35]. The weakly bound neutron $3p$ and, to a lesser extent, the $2f$ orbits deviate from the linear proportionality, with the largest reduction shown by the $3p$ data. The $^{208}$Pb energy splittings presented in Fig. 4 (b) illustrate the same effect. In this case, it is the weakly bound $3d$ neutron orbits that exhibit the largest deviation.

The observed splittings are well reproduced by the calculations labeled “Woods–Saxon”, performed using the potential of Eq. (1), with $r_0 = 1.27$ fm, $a = 0.67$ fm, and the Bohr and Mottelson parameterization of $V_0$ and $V_{ls}$ for neutron orbits, i.e. $V_0 = -51 + 33(N - Z)/A$ MeV and $V_{ls} = CV_0$ [4], where the symbols take their usual meanings. $C$ is an isotope-specific normalization constant, and is approximately $-0.44$ in medium-heavy nuclei [4]. In this work, its value was determined from the $\Delta_{so}$ of the strongly bound orbits, yielding $C = -0.3344$ and $C = -0.3168$ respectively in $^{132}$Sn and $^{208}$Pb. In the calculations, the bare nucleon mass, 940 MeV/$c^2$, was employed. The theoretical $\Delta_{so}$ were obtained from the binding energies of the calculated wavefunctions. The agreement is remarkable, since in the calculations both the central and the SO potential strengths are the same for all orbits.

In addition to the neutron data, it is interesting to point out that, assuming a single-proton configuration for the low-lying states in $^{133}$Sb and $^{131}$In, the $\Delta_{so}$ of the strongly bound proton $2p$ and $2d$ orbits in $^{131}$Sn (respectively 988 [32] and 1680 keV [54] inferred from $\gamma$-ray spectroscopy measurements), would also lie close to the straight line in Fig. 4 (a). The same observation holds true for the strongly bound $2d$ proton-orbit in $^{208}$Pb.

The dependence of $\Delta_{so}/(\ell + 1/2)$ on the binding energy of individual orbits was calculated by varying the depth of the central potential $V_0$, keeping $V_{ls}$ unchanged, and it is shown for $^{132}$Sn and $^{208}$Pb, respectively in Fig. 4 (c) and (d), where the symbols correspond to the experimental data. The calculations illustrate that $\Delta_{so}/(\ell + 1/2)$ is nearly constant for strongly bound orbits, and rapidly decreases when the binding energy is less than $\sim$ 3 MeV, with the largest drop shown by the low-$\ell$ orbits. Due to the weak

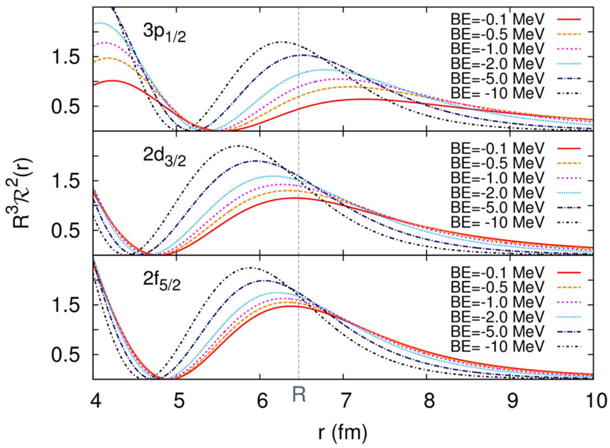


**Fig. 5.** The quantity $R^3\mathscr{R}^2(r)$ plotted as a function of $r$ for the $3p_{1/2}$, $2d_{3/2}$ and $2f_{5/2}$ neutron wavefunctions in $^{132}$Sn, calculated for different binding energies. The nuclear mean radius $R$ is indicated by the vertical line. See text for details.

binding and the low centrifugal barrier, the wavefunctions of low-$\ell$ orbits extend far outside the nucleus and are characterized by large r.m.s. radii and lower radial amplitude ($\mathscr{R}(r)$) at the nuclear surface (this is true also for $s$ orbits). This is illustrated in Fig. 5, where the binding-energy dependence of the quantity $R^3\mathscr{R}^2(r)$ is plotted as a function of $r$ for the $j_<$ partners of $^{132}$Sn neutron orbits. Being less bound, generally the $j_<$ partners have more extended wavefunctions, but the equivalent plot for the $j_>$ orbits looks very similar. While for the $d$ and $f$ orbits, the value of $R^3\mathscr{R}^2(R)$ is nearly 1.4, its strong decrease for the $p$ orbit is the primary cause of the reduced SO splitting, according to Eq. (3). The calculated r.m.s. radii of neutron wavefunctions in $^{132}$Sn are, respectively, 7.48 ($3p_{3/2}$), 8.29 ($3p_{1/2}$), 5.32 ($2d_{5/2}$), 5.34 ($2d_{3/2}$), 6.21 ($2f_{7/2}$), and 6.83 ($2f_{5/2}$) fm, compared to a mean radius $R = 6.47$ fm. The different radial shapes of $j_>$ and $j_<$ orbits cause an additional small reduction of the SO energy splitting, but the main effect is linked to the decrease of $R^3\mathscr{R}^2(r)$ at the nuclear surface.

The remarkable match between data and calculations provides direct evidence that the SO potential is dominated by the surface derivative, which leads to a reduction of the energy splitting of the weakly bound low-$\ell$ orbits. This evidence impacts on the current discussion on the possible weakening of the SO interaction in exotic, neutron-rich nuclei. Unlike previous experimental works [15,16] where the reduction of SO energy splitting in neutron-rich nuclei was examined by comparing different isotopes, the analysis of the different $\Delta_{so}$ of strongly and weakly bound orbits belonging to the same doubly magic nucleus dispenses with uncertainties linked to the comparison of different systems.

In conclusion, neutron-hole states in $^{131}$Sn were populated using the $^{132}$Sn(d, t) single-neutron pick-up reaction in inverse kinematics. The experimental spectroscopic factors extracted via DWBA analysis revealed large occupancies of all single-hole states populated, confirming the robust character of the $N = 82$ shell closure. The energy splitting of the neutron $2d_{3/2}$ and $2d_{5/2}$ SO partners in $^{131}$Sn was extracted and examined together with those of $3p$ and $2f$ in $^{133}$Sn [17,19], revealing a $\sim 50\%$ lower $\Delta_{so}/(\ell + 1/2)$ for the weakly bound $3p$ orbits. The SO energy splittings can all be reproduced remarkably well by one-body potential calculations similar to those of Refs. [12,16], using the same SO potential strength for all orbits. This measurement shows that a large reduction of SO energy splittings can arise from the extended radial wavefunctions of weakly bound orbits, without invoking a weakening of the SO strength. The comparison of different SO-partner orbits in the same neutron-rich nucleus gives a new viewpoint to investigate changes of the SO interaction. This work is the first consistent study of the SO splitting of deeply and weakly bound orbits in the same nucleus (being an exceptionally good doubly magic nucleus helps minimize uncertainties pertaining to the energies of single-particle orbits), studied under essentially identical conditions (beam energy, facility, instrumentation), and applied away from stability in the vicinity of $r$-process nucleosynthesis.

Reduced SO energy splittings can be expected to occur also in nuclei in still unexplored regions of the nuclear chart, which in turn impacts nuclear astrophysics. As many of the relevant $r$-process nuclei are currently inaccessible to spectroscopic study, it is crucial to reliably predict their neutron-capture cross sections. Correctly accounting for the SO energy splitting in loosely bound neutron-rich systems is in fact critical to predicting the energies and ordering of the low-$\ell$ states which drive the DSD neutron-capture cross sections. Finally, in order to further examine the SO splitting of proton orbits, it is important that single-particle and single-hole states in $^{133}$Sb and $^{131}$In are studied via transfer and/or knock-out reactions. While the purity and intensity of post-accelerated $^{132}$Sn at HRIBF are as yet unmatched, the advances in radioactive-ion-beam production will hopefully enable these measurements before long. Fast nucleon-removal reactions on a light target, such as those of Ref. [55], may offer an alternative approach to obtain the required information in future studies.

## Acknowledgements

This work was supported by the Spanish Project MEC Consolider – Ingenio 2010, Project No. CDS2007-00042 (CPAN), the Spanish Ministerio de Economía y Competitividad under contract FPA2014-57196-C5-4-P, the Japan Society for the Promotion of Science (JSPS) KAKENHI Grant Number 26887048 and 15K05094, by the U.S. Department of Energy, Office of Science, Office of Nuclear Physics under Contract No. DE-AC05-00OR22725 (ORNL) and Award Numbers DE-FG52-08NA28552 (Rutgers), DE-SC0001174 (UTK), DE-FG02-96ER40963 (UTK), DE-FG02-96ER40955 (TTU), the U.S. Department of Energy, National Nuclear Security Administration Stewardship Science Academic Alliance under Award Number DE-NA0002132 (Rutgers), the National Science Foundation under Contract No. NSF-PHY-1067906 and NSF-PHY-1404218 (Rutgers). J.A.T. acknowledges the support of the Science and Technology Facilities Council (UK) grants ST/L005743 and ST/L005808/1. This research used resources of the Holifield Radioactive Ion Beam Facility, which was a DOE Office of Science User Facility (HRIBF) operated by the Oak Ridge National Laboratory. The authors are grateful to the HRIBF facility operations staff who made the measurements possible.

## References


[1] G.E. Uhlenbeck, S. Goudsmit, Nature 117 (1926) 264.
[2] F. Kuemmeth, et al., Nature 452 (2008) 448–452.
[3] V. Galitski, Ian B. Spielman, Nature 494 (2013) 49–54.
[4] A. Bohr, B.R. Mottelson, Nuclear Structure, vol. 1, W. A. Benjamin Inc., 1969, p. 218, 238–239.
[5] M. Goeppert Mayer, Phys. Rev. 75 (1949) 1969;
O. Haxel, J.H.D. Jensen, H.E. Suess, Phys. Rev. 75 (1949) 1766.
[6] A. Gade, T. Glasmacher, Prog. Part. Nucl. Phys. 60 (2008) 161.
[7] O. Sorlin, M.-G. Porquet, Prog. Part. Nucl. Phys. 61 (2008) 602.
[8] R. Kanungo, Phys. Scr. T 152 (2013) 014002.
[9] T. Otsuka, T. Suzuki, R. Fujimoto, H. Grawe, Y. Akaishi, Phys. Rev. Lett. 95 (2005) 232502.
[10] K. Karakatsanis, et al., Phys. Rev. C 95 (2017) 034318.
[11] M. Kohno, Phys. Rev. C 86 (2012), 061301(R).
[12] I. Hamamoto, et al., Nucl. Phys. A 683 (2001) 255.
[13] J.P. Schiffer, et al., Phys. Rev. Lett. 92 (2004) 162501.
[14] T. Otsuka, Phys. Scr. T 152 (2013) 014007.
[15] G. Burgunder, O. Sorlin, et al., Phys. Rev. Lett. 112 (2014) 042502.
[16] B.P. Kay, C.R. Hoffman, A.O. Macchiavelli, Phys. Rev. Lett. 119 (2017) 182502.
[17] K.L. Jones, et al., Nature 465 (2010) 454.

[18] K.L. Jones, et al., Phys. Rev. C 84 (2011) 034601.
[19] P. Hoff, et al., Phys. Rev. Lett. 77 (1996) 1020.
[20] R.L. Kozub, et al., Phys. Rev. Lett. 109 (2012) 172501.
[21] J.M. Allmond, et al., Phys. Rev. Lett. 112 (2014) 172701.
[22] B.M. Manning, Ph.D. Thesis, University of Rutgers, retrieved from https://doi.org/10.7282/T3GF0S64.
[23] S.D. Pain, et al., PoS (NIC X) 142 (2008).
[24] J.S. Thomas, et al., Phys. Rev. C 71 (2005) 021302.
[25] J.S. Thomas, et al., Phys. Rev. C 76 (2007) 044302.
[26] S. Ahn, Ph.D. diss.. University of Tenessee, 2013, retrieved from http://trace.tennessee.edu/utk_graddiss/2392.
[27] R. Orlandi, et al., Phys. Lett. B 740 (2015) 298.
[28] R. Orlandi, Acta Phys. Pol. B 47 (2016) 803.
[29] B. Fogelberg, et al., Phys. Rev. C 70 (2004) 034312.
[30] M. Sanchez-Vega, et al., Phys. Rev. Lett. 80 (1998) 5504.
[31] B. Fogelberg, Y. Zongyuan, L. Spanier, Phys. Lett. B 209 (1988) 173.
[32] J. Taprogge, et al., Phys. Rev. Lett. 112 (2014) 132501.
[33] M.R. Mumpower, R. Surman, G.C. McLaughlin, A. Aprahamian, Prog. Part. Nucl. Phys. 86 (2016) 86–126.
[34] S. Chiba, et al., Phys. Rev. C 77 (2008) 015809.
[35] M. Wang, G. Audi, et al., Chin. Phys. C 36 (2012) 1603.
[36] Yu. Khazov, A.A. Rodionov, S. Sakharov, B. Singh, Nucl. Data Sheets 104 (2005) 497.
[37] K.T. Schmitt, et al., Phys. Rev. C 88 (2013) 064612.
[38] M. Febbraro, et al., Nucl. Instrum. Methods Phys. Res., Sect. B 410 (2017) 53.
[39] D.W. Bardayan, et al., Nucl. Instrum. Methods Phys. Res., Sect. A 711 (2013) 160.
[40] S.D. Pain, et al., Nucl. Instrum. Methods Phys. Res., Sect. A 261 (2007) 1122.
[41] Yu. Khazov, I. Mitropolsky, A. Rodionov, Nucl. Data Sheets 107 (2006) 2715.
[42] J.A. Tostevin, University of Surrey version of the code TWOFNR (of M. Toyama, M. Igarashi and N. Kishida).
[43] P.J.A. Buttle, L.J.B. Goldfarb, Proc. Phys. Soc. 83 (1964) 701.
[44] B.F. Gibson, D.R. Lehman, Phys. Rev. C 29 (1984) 1017.
[45] I. Borbély, P. Doleschall, Phys. Lett. B 113 (1983) 443.
[46] F. Perey, B. Buck, Nucl. Phys. 32 (1962) 353.
[47] W.W. Daehnik, J.D. Childs, Z. Vrcelj, Phys. Rev. C 21 (1980) 2253.
[48] C.M. Perey, F.G. Perey, At. Data Nucl. Data Tables 17 (1976) 1.
[49] H. Hashimoto, Nucl. Phys. A 471 (1987) 520, data retrieved from the EXFOR database, entry E1367.029.
[50] S.E. Vigdor, R.D. Rathmell, H.S. Liers, W. Haeberli, Nucl. Phys. A 210 (1973) 70.
[51] J.M. Lohr, W. Haeberli, Nucl. Phys. A 232 (1974) 381.
[52] C.M. Perey, F.G. Perey, Phys. Rev. 32 (1963) 755.
[53] E.R. Flynn, et al., Phys. Rev. 182 (1969) 1113.
[54] V.I. Izakov, et al., Eur. Phys. J. A 14 (2002) 29.
[55] V. Vaquero, et al., Phys. Rev. Lett. 118 (2017) 202502.